Smart Structures and Systems, *Vol. 17, No. 6 (2016) 935-956*
DOI: http://dx.doi.org/10.12989/sss.2016.17.6.935

Image-based structural dynamic displacement measurement using different multi-object tracking algorithms

X.W. Ye*, C.Z. Dong and T. Liu

Department of Civil Engineering, Zhejiang University, Hangzhou 310058, China

(Received December 31, 2015, Revised April 3, 2016, Accepted April 8, 2016)

Abstract. With the help of advanced image acquisition and processing technology, the vision-based measurement methods have been broadly applied to implement the structural monitoring and condition identification of civil engineering structures. Many noncontact approaches enabled by different digital image processing algorithms are developed to overcome the problems in conventional structural dynamic displacement measurement. This paper presents three kinds of image processing algorithms for structural dynamic displacement measurement, i.e., the grayscale pattern matching (GPM) algorithm, the color pattern matching (CPM) algorithm, and the mean shift tracking (MST) algorithm. A vision-based system programmed with the three image processing algorithms is developed for multi-point structural dynamic displacement measurement. The dynamic displacement time histories of multiple vision points are simultaneously measured by the vision-based system and the magnetostrictive displacement sensor (MDS) during the laboratory shaking table tests of a three-story steel frame model. The comparative analysis results indicate that the developed vision-based system exhibits excellent performance in structural dynamic displacement measurement by use of the three different image processing algorithms. The field application experiments are also carried out on an arch bridge for the measurement of displacement influence lines during the loading tests to validate the effectiveness of the vision-based system.

Keywords: structural health monitoring; displacement measurement; vision-based system; digital image processing; pattern matching algorithm; mean shift tracking algorithm

1. Introduction

Structural health monitoring (SHM) of civil infrastructure aims to measure the environmental and operational parameters and observe the static and dynamic structural features, and then to execute the structural condition and safety evaluation and give the instructive inspection and maintenance recommendations (Ni *et al*. 2010, Ni *et al*. 2012). In an SHM system, different kinds of sensors are applied to acquire a variety of continuous monitoring data characterizing the physical quantities of the instrumented structure, and thus the novel data-driven structural condition assessment approaches can be developed to carry out the diagnostic and prognostic tasks. In this way, the limitations and drawbacks existent in the traditional visual inspection are able to be resolved (Ye *et al*. 2012). With the development of photography techniques, the cameras with high resolution and speed are becoming more and more popular and convenient to be employed for

*Corresponding author, Associate Professor, E-mail: cexwye@zju.edu.cn

http://www.techno-press.org/?journal=sss&subpage=8 ISSN: 1738-1584 (Print), 1738-1991 (Online)

industrial measurement. Various types of cameras and lenses are available for different purposes in the corresponding areas. The structural evaluation indices can be constructed based on the images captured by the image acquisition devices with the aid of image processing algorithms. In these quantitative indices, the structural displacement is one of the key structural performance indicators for structural safety condition evaluation and health state prediction (Ye *et al*. 2013, Ye *et al*. 2015).

Recently, the vision-based structural dynamic displacement measurement has attracted increasing attentions from the researchers and engineers participated in the SHM practice (Jauregui *et al*. 2003, Park *et al*. 2010, Feng *et al*. 2015, Henke *et al*. 2015). Olaszek (1999) presented a vision method which made it possible to measure the structural displacement of the bridge structure under static and dynamic loads. Wahbeh *et al*. (2003) developed a novel vision-based approach for realizing direct measurement of the absolute displacement time history at selectable locations of engineering structures. Ji and Chang (2007, 2008) used an optical flow method to determine the displacement of cable vibration, and presented a nontarget stereo vision technique based on the subpixel edge detection algorithm to measure the response of a line-like structure in both spatial and temporal domains. Ho *et al*. (2012) developed a synchronized multi-point vision-based system for displacement measurement of civil infrastructure. Fukuda *et al*. (2013) proposed a robust object search algorithm for accurate displacement measurement by tracking existing features on the structure without requiring a conventional target panel installed on the structure and proposed a subpixel technique to reduce the measurement error. Guo and Zhu (2016) proposed a modified inverse compositional algorithm to reduce the computation time of the Lucas-Kanade template tracking algorithm, and improved the efficiency of vision method in remote structural dynamic displacement measurement.

In this paper, the vision-based structural dynamic displacement measurement based on three different kinds of methods, i.e., the grayscale pattern matching (GPM) algorithm, the color pattern matching (CPM) algorithm, and the mean shift tracking (MST) algorithm are presented. An advanced noncontact multi-point structural displacement measurement system is developed by integrating the image acquisition device with the proposed image processing algorithms. A series of laboratory tests are conducted to investigate the feasibility and effectiveness of the developed vision-based system in multi-point structural dynamic displacement measurement. The results obtained from the vision-based system are compared with those simultaneously measured by the magnetostrictive displacement sensor (MDS). The comparative study and statistical error analysis reveal that the developed vision-based system is robust in multi-point structural dynamic displacement measurement with the aid of the three different image processing algorithms. The effectiveness of the vision-based system is also validated through field application experiments carried out on an arch bridge for the measurement of displacement influence lines during the loading tests.

2. Multi-object tracking algorithms for structural dynamic displacement measurement

2.1 Grayscale pattern matching (GPM) algorithm

To obtain the structural displacements of the predefined targets on the structure, the digital camera is used to capture the grayscale images in which all the predefined targets are contained. The patterns are extracted from the first grayscale image and migrated in the following grayscale

images captured by the digital camera. Fig. 1 illustrates the schematic diagram of the grayscale pattern matching algorithm (Ye *et al*. 2013, Ye *et al*. 2015). The sub-image is fetched to represent the pattern $f_k(x, y)$ with a size of $m_k \times n_k$ in the initial image $g^0(x, y)$ with a size of $M \times N$. Here, k is the number of the patterns. The initial coordinate of the center point of the kth pattern is denoted as (x_k^0, y_k^0). The normalized correlation coefficient $c_k(i, j)$ between the pattern $f_k(x, y)$ and the image $g^t(x, y)$ at the point (i_k, j_k) is given by

$$\alpha_k(i,j)=\frac{\sum_{x=0}^{M-1}\sum_{y=0}^{N-1}\left(f_k(x,y)-\overline{f_k}\right)\left(g^t(x+i,y+j)-\overline{g^t}\right)}{\left(\sum_{x=0}^{M-1}\sum_{y=0}^{N-1}\left(f_k(x,y)-\overline{f_k}\right)\right)^{\frac{1}{2}}\left(\sum_{x=0}^{M-1}\sum_{y=0}^{N-1}\left(g^t(x+i,y+j)-\overline{g^t}\right)\right)^{\frac{1}{2}}} \tag{1}$$

where $i = 0, 1, ..., M-1$, $j = 0, 1, …, N-1$, t is the time on which the image is captured, $\overline{f_k}$ is the average grayscale value of the pattern $f_k(x, y)$, and $\overline{g_k}$ is the average grayscale value of the overlapped region between the pattern $f_k(x, y)$ and the image $g^t(x, y)$. Assuming that the original image $g^t(x, y)$ is at the top left corner, the correlation computation is the process of moving the pattern $f_k(x, y)$ on the image and calculating the normalized correlation coefficient $c_k(i, j)$. The grayscale value of each pixel in the pattern is multiplied by that in the overlapped region of the image, and the calculation task is executed for the overlapped region between $f_k(x, y)$ and $g^t(x, y)$. The maximum value of $\alpha_k(i, j)$ indicates that the pattern $f_k(x, y)$ best matches the overlapped region of the image $g^t(x, y)$ and the target position is identified. The coordinate of the center point of this overlapped region is represented by (x^t_k, y^t_k).

When the best pattern matching status is accomplished in the image coordinate, it is required to convert the change of the target position in the image to the actual structural displacement. If there are d pixels in the vertical direction for the target in the image and the actual size of the target in the vertical direction is D, and then the scale ratio r can be calculated by

$$r=\frac{D}{d} \tag{2}$$

After obtaining the initial coordinate of the center point of the kth pattern (x_k^0, y_k^0) and the coordinate of the center point of the overlapped region (x^t_k, y^t_k), the horizontal structural displacement $x_k(t)$ and the vertical structural displacement $y_k(t)$ of the kth target can be derived by

$$\begin{bmatrix} x_k(t) \\ y_k(t) \end{bmatrix} = r \begin{bmatrix} x_k^t & x_k^0 \\ y_k^t & y_k^0 \end{bmatrix} \begin{bmatrix} 1 & 1 \\ -1 & -1 \end{bmatrix} \tag{3}$$

2.2 Color pattern matching (CPM) algorithm

The flowchart of structural dynamic displacement measurement based on the color pattern matching algorithm is illustrated in Fig. 2. The image in RGB or HSV format is captured by the digital color camera. The patterns are extracted from the first image and the initial pixel locations of the patterns are recorded. The color information in the predefined patterns and the succeeding images transferred by the image sequence is explored. The basic operation is to move the patterns

across the images pixel by pixel and compares the color information at certain location of the images with that of the patterns. A list of possible matches with scores via a coarse to fine search strategy are found by calculating the similarity between the patterns and the images based on the color pattern matching algorithm. Each match location is refined by use of a hill climbing process (Russell and Norvig 2010). When the scores reach the maximum values, the best pattern match results are obtained and the locations of the matched areas are acquired. By multiplying the scale ratio with the pixel locations, the structural dynamic displacements of the targets are achieved. Here the pixel locations refer to the pixel coordinates, and the scale ratio can be calculated by the method stated in Section 2.1. The displacement time histories of the targets will be obtained if the steps in the task cycle are repeated.

Fig. 3 illustrates the flowchart of the similarity calculation in the color pattern matching algorithm. During the matching phase, the color spectrum obtained from each succeeding image is compared with the reference color spectrum of each pattern during the learning step. A match score is computed based on the similarity evaluation between these two color spectra by the Manhattan distance (Perlibakas 2004). A fuzzy weighting function is applied to the color spectra before computing the distance between the two vectors (Mansoori *et al*. 2007). The absolute difference between the pattern and the region of the image is indicated; meanwhile a normalized match score ranging from 0 to 1 is obtained. The best match is accomplished with the maximum match score.

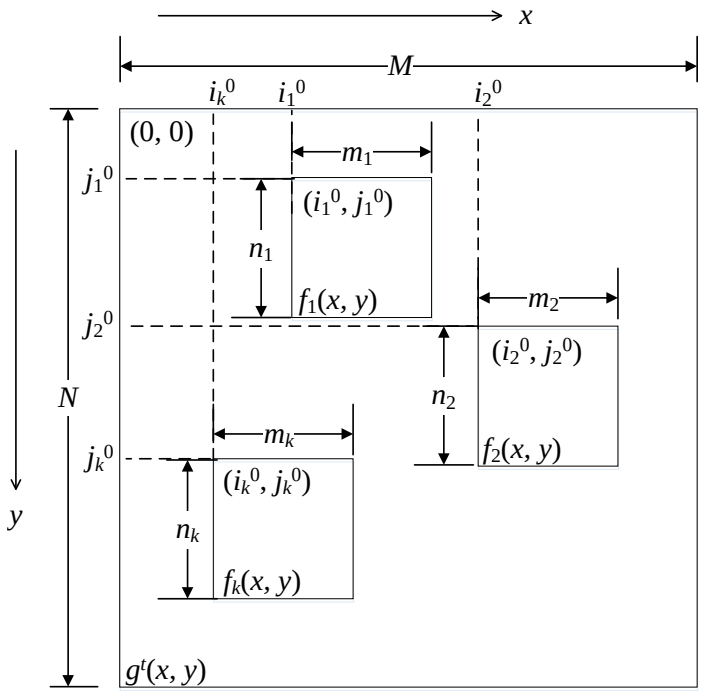

Fig. 1 Schematic diagram of grayscale pattern matching algorithm

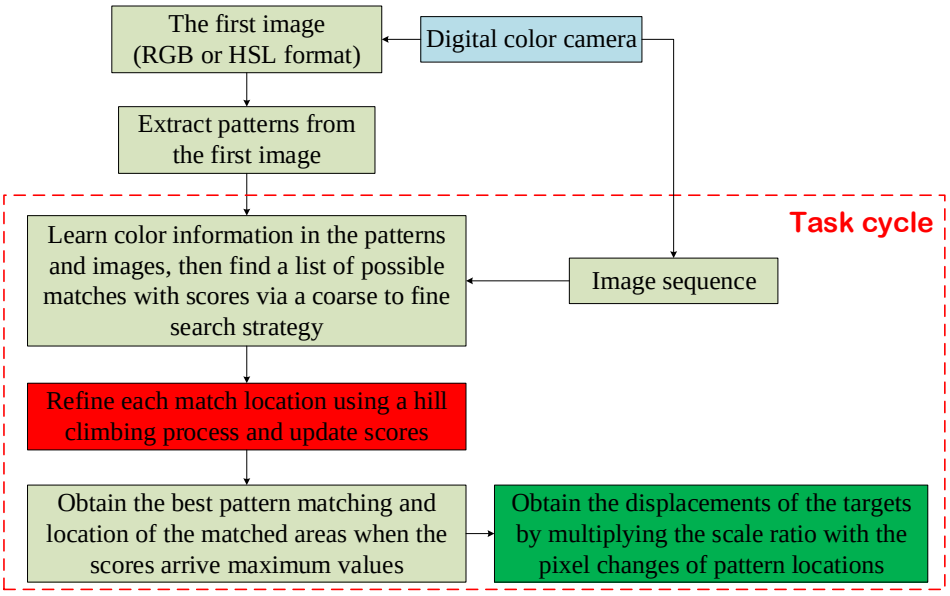

Fig. 2 Flowchart of structural dynamic displacement measurement based on color pattern matching algorithm

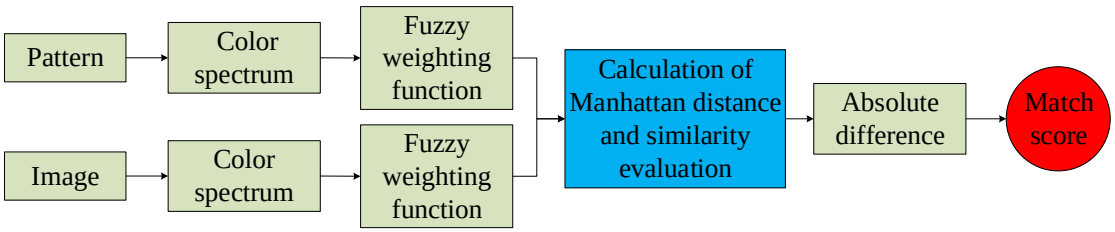

Fig. 3 Flowchart of similarity calculation in color pattern matching algorithm

2.3 Mean shift tracking (MST) algorithm

Alike the framework proposed in Sections 2.1 and 2.2, the mean shift tracking algorithm also needs to characterize the target and choose a feature space for characterizing the pattern. The reference target model is represented by its probability distribution function (PDF) q in the feature space. The reference model can be chosen as the color or grayscale PDF of the target. After capturing the first image by the digital camera, the target can be considered to be centered at the spatial location $\mathbf{0}(0, 0)$, the origin relative to the target in the succeeding images. $\{\boldsymbol{s}_i^*\}_{i=1...\mu}$ is the pixel locations in the region defined as the target model. In the succeeding image, a target candidate is defined at the location $\boldsymbol{l}$, and is characterized by the PDF $p(\boldsymbol{l})$. Because the digital image is described by a discrete form, in the actual operation, η-bin histograms are used. Then the PDF of the target model is represented by

$$\boldsymbol{q} = \{q_u\}_{u=1\ldots\eta} \qquad \sum_{u=1}^{\eta} q_u = 1 \tag{4}$$

The target candidate is expressed by

$$\boldsymbol{p} = \{p_u\}_{u=1\ldots\eta} \qquad \sum_{u=1}^{\eta} q_u = 1 \tag{5}$$

A kernel function $K(s)$ is introduced to assign smaller weights to pixels farther from the center of the target. Using these weights can increase the robustness of the density estimation since the peripheral pixels are often affected by the interference factors from the background (Comaniciu *et al.* 2003). The probability of the feature u in the target model is then calculated as

$$q_u = C\sum_{i=1}^{\mu} K\left(\left\|\boldsymbol{s}_i^*\right\|^2\right)\delta\left[b\left(\boldsymbol{s}_i^*\right) - u\right] \tag{6}$$

where C is the normalization constant derived by

$$C = \frac{1}{\sum_{i=1}^{\mu} K\left(\left\|\boldsymbol{s}_i^*\right\|^2\right)} \tag{7}$$

Given b: $R^2 \rightarrow \{1\ldots\eta\}$, let $\boldsymbol{b}(\boldsymbol{s}_i^*)$ refer to the color or grayscale index of bins to the pixel at the location $\boldsymbol{s}_i^*$. δ is the Kronecker delta function.

Similarly, the probability of the feature u in the target candidate is given by

$$p_u(\boldsymbol{l}) = C_h\sum_{i=1}^{\mu_h} K\left(\left\|\frac{\boldsymbol{l}-\boldsymbol{s}_i}{h}\right\|^2\right)\delta\left[b(\boldsymbol{s}_i) - u\right] \tag{8}$$

where $\{\boldsymbol{s}_i\}$(i=1... μ_h) is the pixel locations of the target candidate which is centered at $\boldsymbol{l}$ in the current image, $K(s)$ is the kernel function with a bandwidth h which is relative to the target scale, and C_h is normalization constant which is calculated by

$$C_h = \frac{1}{\sum_{i=1}^{\mu_h} K\left(\left\|\frac{\boldsymbol{l}-\boldsymbol{s}_i}{h}\right\|^2\right)} \tag{9}$$

With the Eqs. (6) to (9), q_u is the kernel probability density estimation of the distribution of the target feature, determining the target location in the current image is to find a location $\boldsymbol{l}$, which makes the similarity between $p_u(\boldsymbol{l})$ and q_u arriving the most. Here the Bhattacharyya coefficient is used to evaluate the similarity between the target and the candidate

$$\rho(\boldsymbol{l}) \equiv \rho[p(\boldsymbol{l}), q] = \sum_{u=1}^{\eta}\sqrt{p_u(\boldsymbol{l})q_u} \tag{10}$$

The locally maximum value of the Bhattacharyya coefficient indicates that the target is found in the current image. The search task for the new target location in the current image starts at the location $\boldsymbol{l}_0$ of the target in the previous image. The linear approximation of the Bhattacharyya

coefficient is obtained by use of the Taylor expansion around the value $p_u(\boldsymbol{l}_0)$

$$\rho[p(\boldsymbol{l}),q]\approx\frac{1}{2}\sum_{u=1}^{\eta}\sqrt{p_u(\boldsymbol{l}_0)q_u}+\frac{1}{2}\sum_{u=1}^{\eta}p_u(\boldsymbol{l})\sqrt{\frac{q_u}{p_u(\boldsymbol{l}_0)}} \tag{11}$$

Substitute Eqs. (6) and (8) into Eq. (11), and then

$$\rho[p(\boldsymbol{l}),q]\approx\frac{1}{2}\sum_{u=1}^{\eta}\sqrt{p_u(\boldsymbol{l}_0)q_u}+\frac{C_h}{2}\sum_{u=1}^{\mu_h}w_iK\left(\left\|\frac{\boldsymbol{l}-\boldsymbol{s}_i}{h}\right\|^2\right) \tag{12}$$

where

$$w_i=\sum_{u=1}^{\eta}\sqrt{\frac{q_u}{p_u(\boldsymbol{l}_0)}}\delta[b(\boldsymbol{s}_i)-u] \tag{13}$$

Because the first summation of Eq. (12) is independent with $\boldsymbol{l}$, the second summation of Eq. (12) has to be maximized, to maximize the Bhattacharyya coefficient. The second summation of Eq. (12) represents the kernel density estimation with the kernel function $K(s)$ at $\boldsymbol{l}$ in the current image and each pixel is weighted by w_i. The problem of searching the optimal target candidate is translated into that of looking for the local extreme value of the PDF, which can be completed by the mean shift iteration. Let

$$\nabla_{\boldsymbol{l}}\rho[p(\boldsymbol{l}),q]=0 \tag{14}$$

the mean shift iteration form is obtained as (Fukunaga and Hostetler 1975, Cheng 1995)

$$\boldsymbol{l}_1=\frac{\sum_{i=1}^{\mu_h}\boldsymbol{x}_iw_ig\left(\left\|\frac{\boldsymbol{l}_0-\boldsymbol{s}_i}{h}\right\|^2\right)}{\sum_{i=1}^{\mu_h}w_ig\left(\left\|\frac{\boldsymbol{l}_0-\boldsymbol{s}_i}{h}\right\|^2\right)} \tag{15}$$

where

$$g(s)=-k'(s) \tag{16}$$

The mean shift iteration starts from the initial location of the target in the previous image and the process is repeated until the problem converges or reaches the maximum iterations. Then the location of the target is obtained in the current image, which is denoted as (x^t_k, y^t_k), here t is the time when the current image is captured and k indicates the kth target. The initial location of the target is denoted as (x_k^0, y_k^0). As described in Section 2.1, with Eqs. (2) and (3) the structural dynamic displacement of the kth target at time t can be obtained.

3. Laboratory experimental study

3.1 Experimental setup

As illustrated in Fig. 4, the system hardware of the vision-based multi-point structural dynamic displacement measurement system consists of a high-resolution industrial camera, a zoom lens, a computer, and a Gigabit Ethernet standard LAN wire. The developed data analysis software is integrated with three different algorithms for target tracking and image processing in execution of vision-based structural dynamic displacement calculation.

In the experimental study, a three-story steel frame model was designed and fabricated which is fixed on the earthquake simulator. Three vision points (P1, P2 and P3) were deployed on the steel frame for structural dynamic displacement measurement, and three magnetostrictive displacement sensors were installed at the same locations for comparative analysis. The vision points are characterized by markers with different colors. The earthquake simulator gives various vibration cases with an amplitude of ±5 mm and different frequencies of 0.5 Hz, 1.0 Hz and 1.5 Hz, respectively. In each vibration scenario, the vision-based system and the MDS simultaneously record the displacement time histories of the three points (P1, P2 and P3). In vision-based structural dynamic displacement measurement, the above-mentioned three algorithms (GPM, CPM and MST) are employed, as listed in Table 1.

Table 1 Experimental scenarios

Case No.	Vision algorithm	Frequency (Hz)	Amplitude (mm)
Case 1	GPM	0.5	±5
Case 2	GPM	1.0	±5
Case 3	GPM	1.5	±5
Case 4	CPM	0.5	±5
Case 5	CPM	1.0	±5
Case 6	CPM	1.5	±5
Case 7	MST	0.5	±5
Case 8	MST	1.0	±5
Case 9	MST	1.5	±5

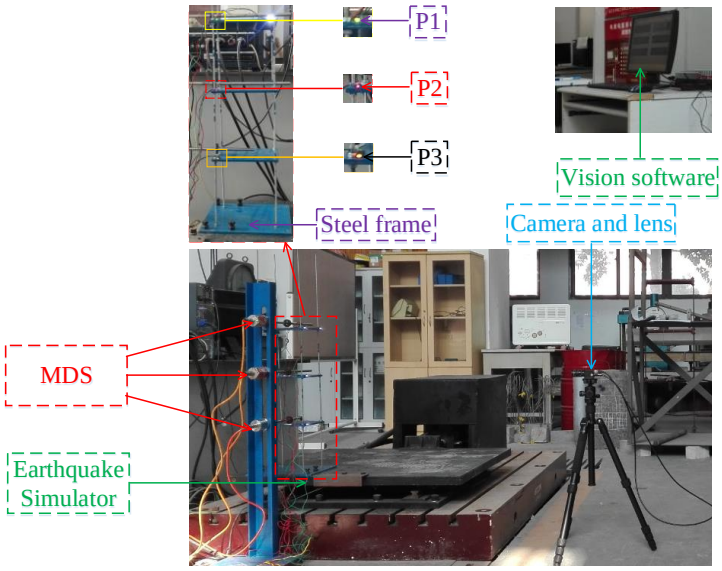

Fig. 4 Experimental setup

3.2 Analysis of experimental results

Figs. 5-7 illustrate the structural dynamic displacements of the three measurement points (P1, P2 and P3) obtained by the vision system with the GPM algorithm-based method and the MDS. The displacement time histories of the three measurement points (P1, P2 and P3) obtained by the two methods are highly consistent on different experimental scenarios (Case 1, Case 2 and Case 3) with various vibration frequencies (0.5 Hz, 1.0 Hz and 1.5 Hz) of the earthquake simulator. The good measurement results are also found in the displacement time histories of the three measurement points (P1, P2 and P3) derived by the CPM and MST algorithms, as illustrated in Fig. 8-13.

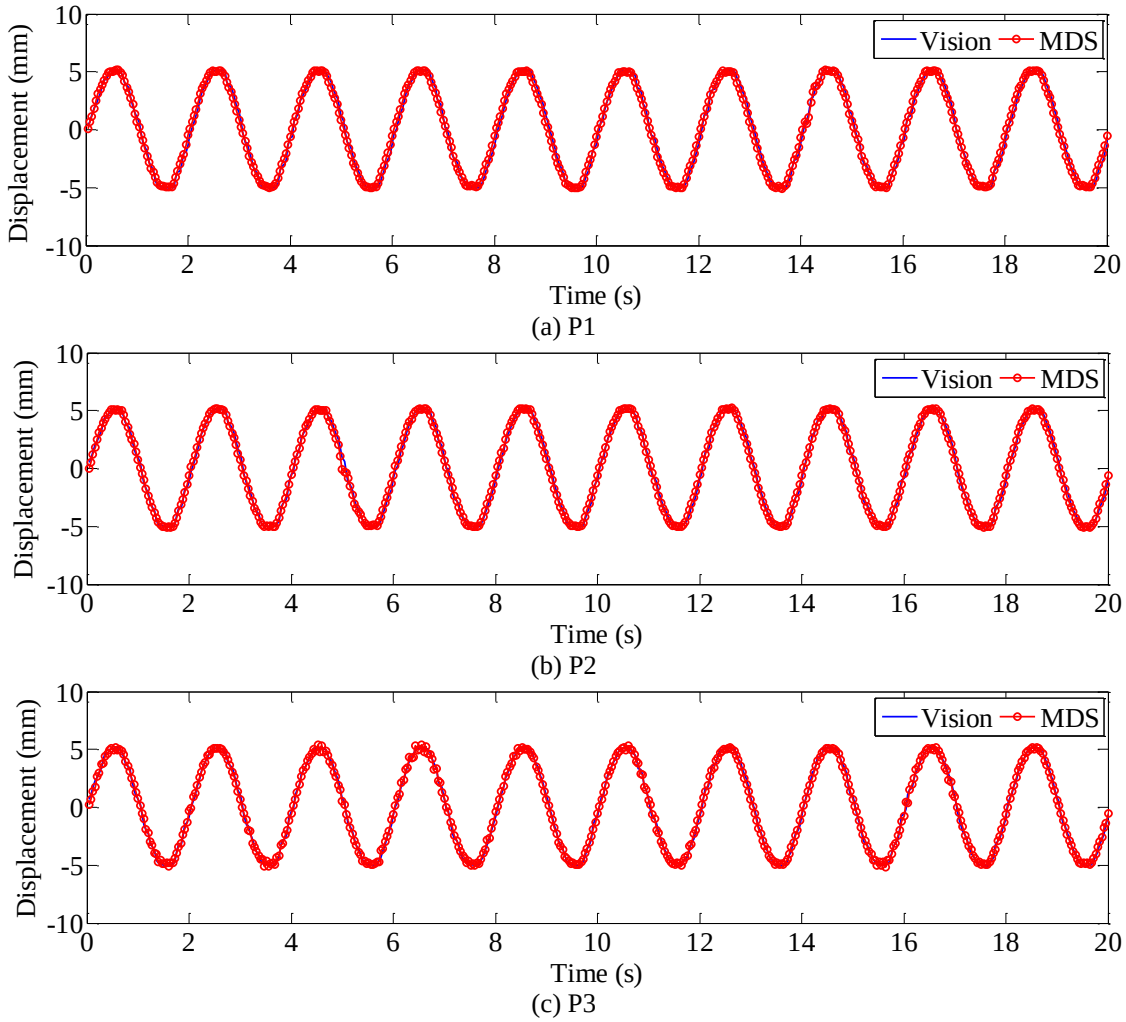

Fig. 5 Comparative analysis of measured displacement results in Case 1

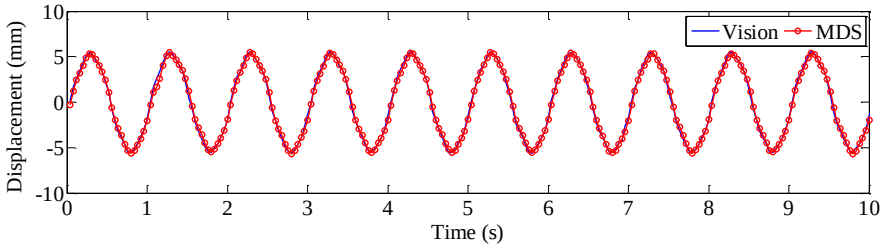

(a) P1

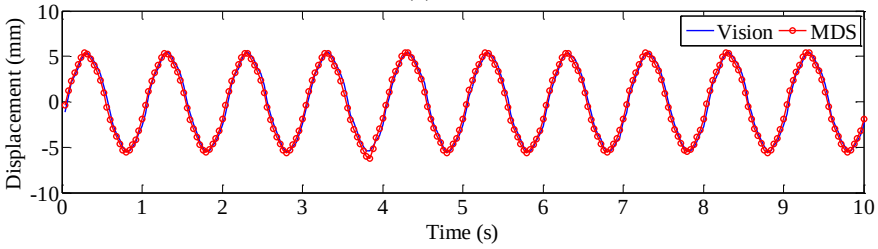

(b) P2

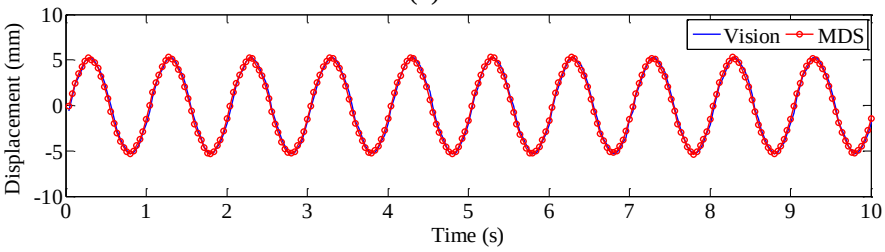

(c) P3

Fig. 6 Comparative analysis of measured displacement results in Case 2

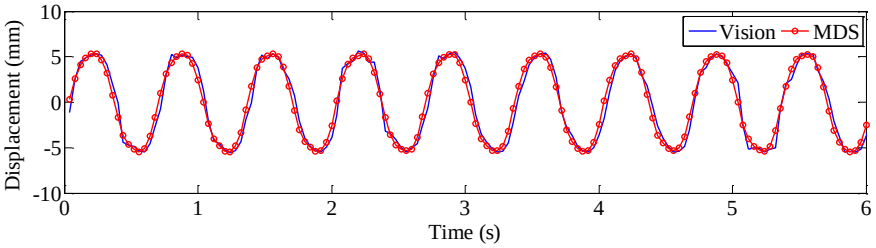

(a) P1

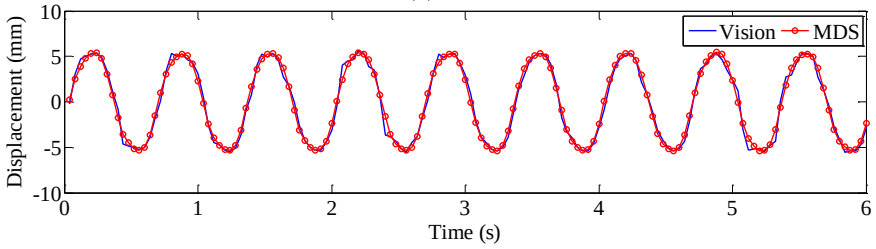

(b) P2

Continued-

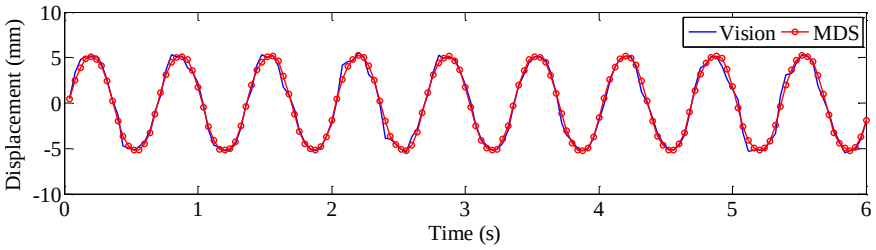

(c) P3

Fig. 7 Comparative analysis of measured displacement results in Case 3

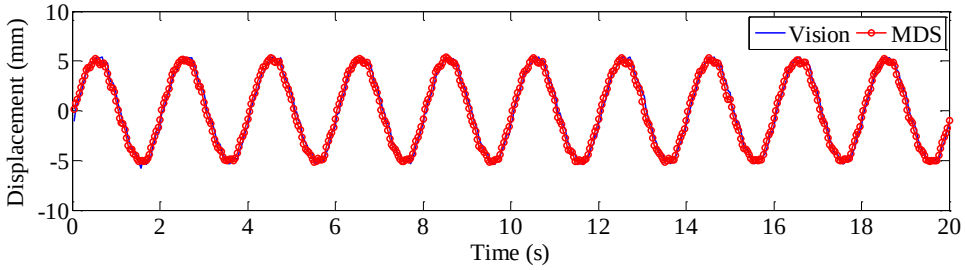

(a) P1

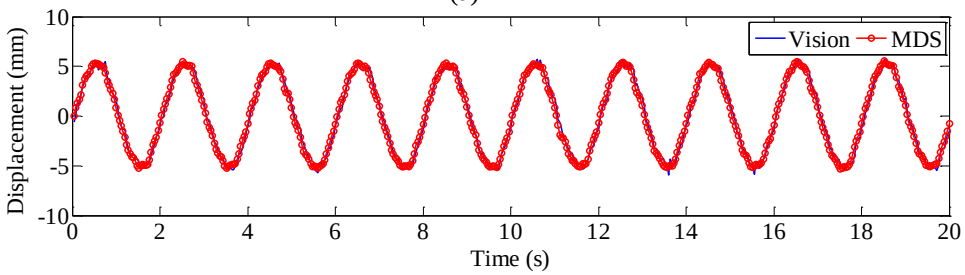

(b) P2

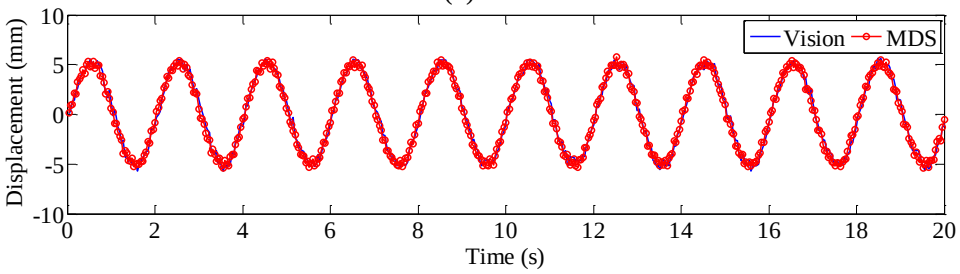

(c) P3

Fig. 8 Comparative analysis of measured displacement results in Case 4

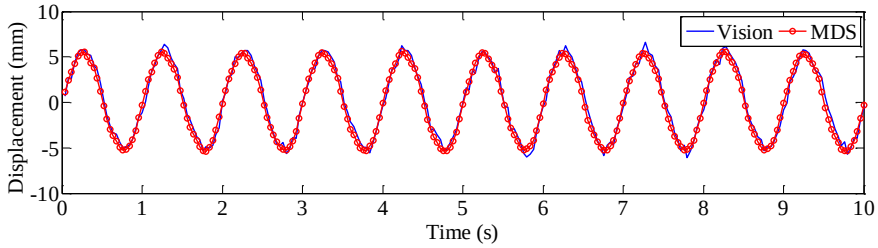

(a) P1

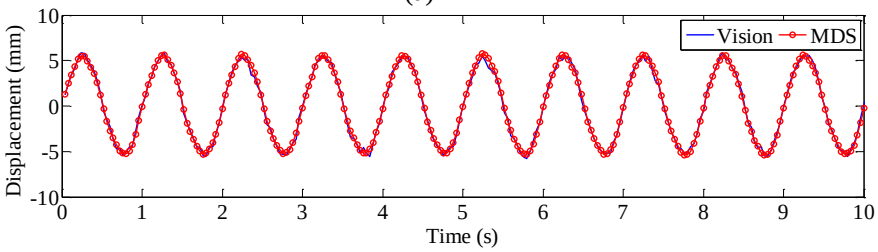

(b) P2

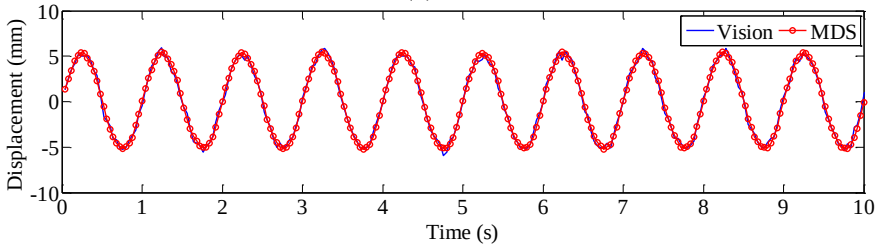

(c) P3

Fig. 9 Comparative analysis of measured displacement results in Case 5

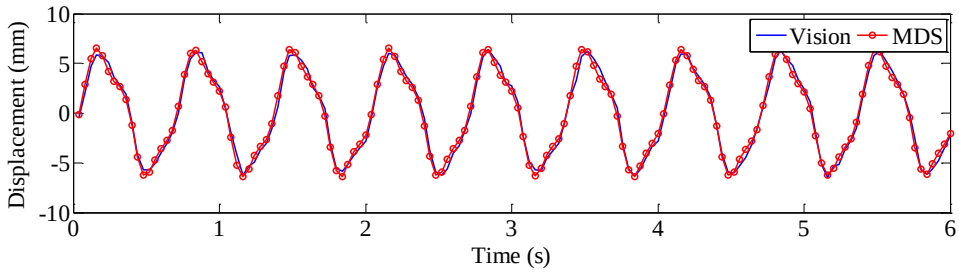

(a) P1

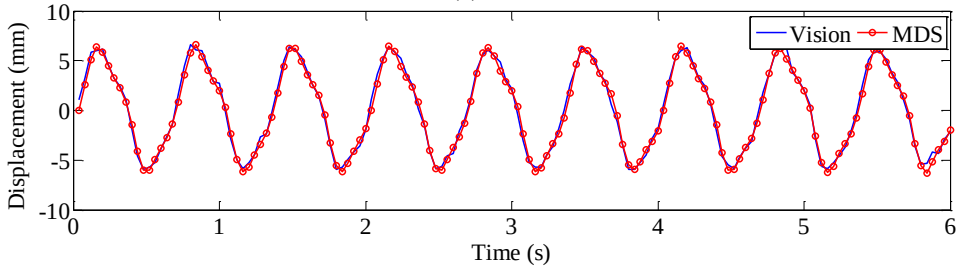

(b) P2

Continued-

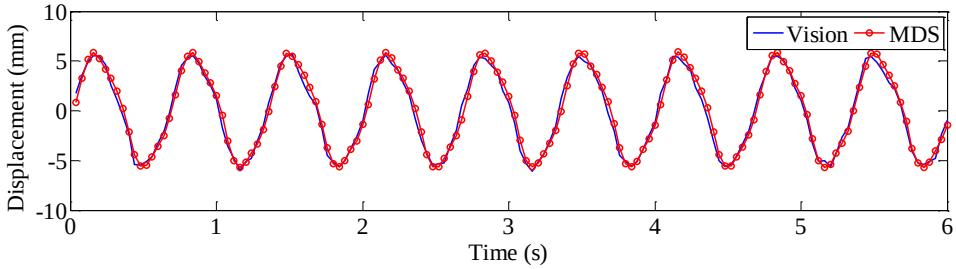

(c) P3

Fig. 10 Comparative analysis of measured displacement results in Case 6

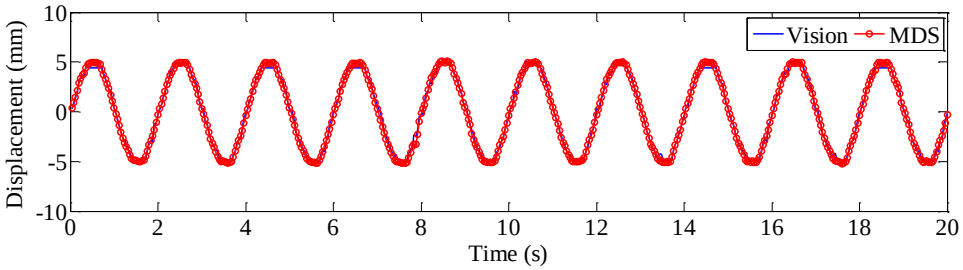

(a) P1

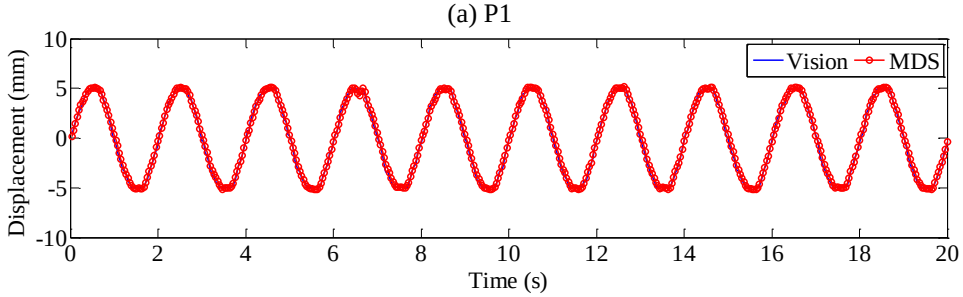

(b) P2

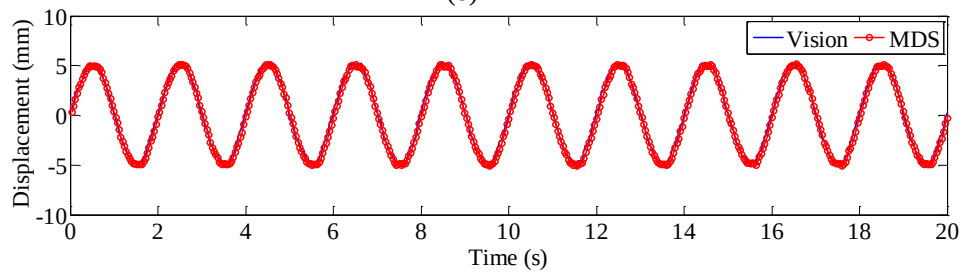

(c) P3

Fig. 11 Comparative analysis of measured displacement results in Case 7

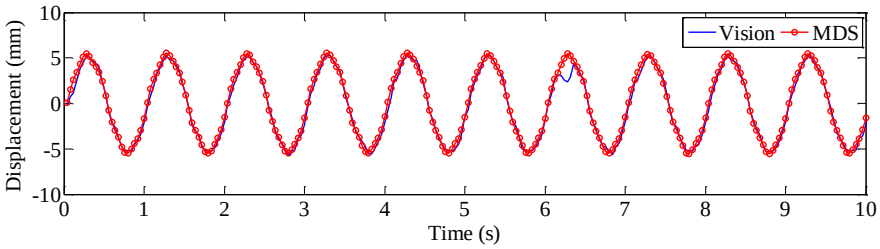

(a) P1

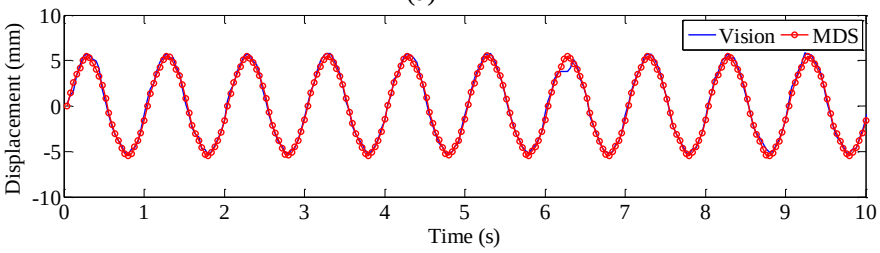

(b) P2

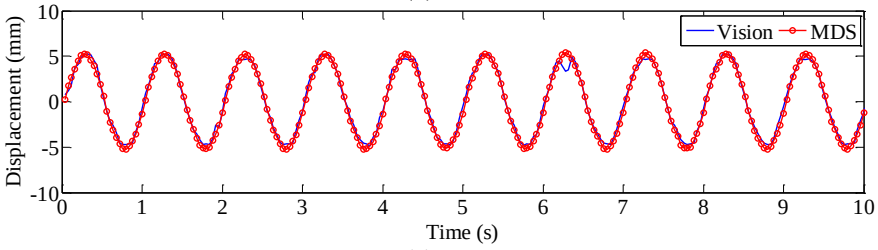

(c) P3

Fig. 12 Comparative analysis of measured displacement results in Case 8

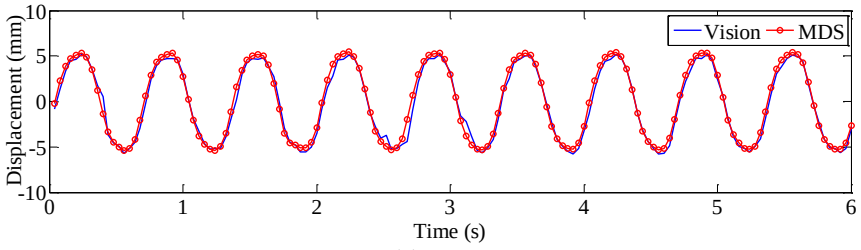

(a) P1

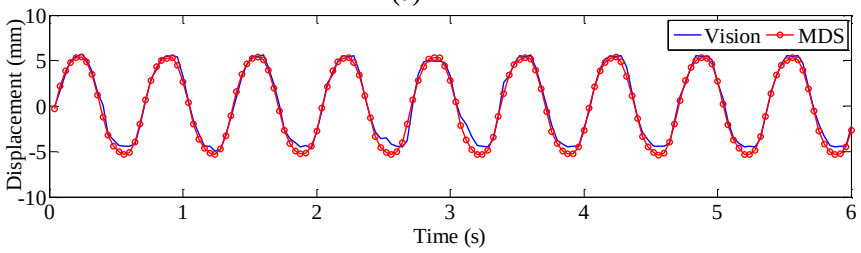

(b) P2

Continued-

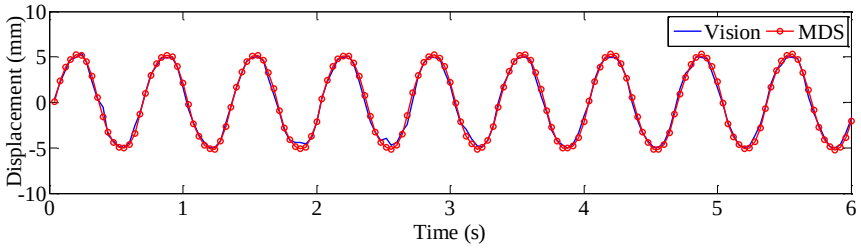

(c) P3

Fig. 13 Comparative analysis of measured displacement results in Case 9

To quantitatively examine the accuracy and stability of these three types of vision-based structural dynamic displacement measurement methods, an error analysis is performed by use of the average of full scale error (AFSE) and the root mean squared full scale error (RMSFSE).

$$\mathrm{AFSE} = \frac{1}{\lambda}\sum_{i=1}^{\lambda}\frac{|v_i - \tau_i|}{\tau_{\max} - \tau_{\min}} \times 100\% \tag{17}$$

$$\mathrm{RMSFSE} = \frac{\sqrt{\frac{1}{\lambda}\sum_{i=1}^{\lambda}(v_i - \tau_i)^2}}{\tau_{\max} - \tau_{\min}} \times 100\% \tag{18}$$

where λ is the number of the measurement data, v_i and τ_i are the ith structural displacement data at time t_i measured by the vision-based system and the MDS, respectively, and $\tau_{\max}$ and $\tau_{\min}$ are the maximum and minimum values of τ_i.

Table 2 lists the statistical error analysis results of the structural dynamic displacement measured by the three different kinds of vision-based structural dynamic displacement measurement methods in reference to those measured by the MDS. It is concluded that the three vision-based methods exhibit good stability and feasibility in structural dynamic displacement measurement with a high extent of accuracy.

Table 2 Results of statistical error analysis

Vision algotithm	Case No.	AFSE (%)			RMSFSE (%)		
		P1	P2	P3	P1	P2	P3
GPM	1	2.6009	1.9468	1.6634	1.9606	1.5035	1.2678
	2	1.9243	3.7383	2.6828	1.4982	2.0238	1.7688
	3	5.6104	3.6307	3.2637	4.9216	3.2634	3.3096
CPM	4	4.1172	3.0622	3.3748	2.5769	2.1418	2.4051
	5	4.5692	2.2140	2.6829	3.0752	1.7026	2.0357
	6	3.3247	2.8817	3.9102	2.1203	2.1582	2.7467
MST	7	2.0771	1.8772	2.8382	1.7119	1.5727	1.9109
	8	2.9758	2.5827	3.0881	3.0598	1.9953	2.5606
	9	3.9290	4.2531	2.7477	3.4819	3.2938	2.2026

4. Field application experiments on an arch bridge

4.1 Description of the arch bridge

The investigated arch bridge with a main span of 130m is located in Hangzhou, China. It is a half-through highway arch bridge. The orthotropic steel deck and steel arch ribs are linked by rigid connections, as illustrated in Fig. 14. The separated abutments and bearing platforms are made up of steel reinforced concrete. The arch system consists of four steel box arch ribs including two main arch ribs and two subarch ribs with an inward inclined angle of 17.5°. The main arch ribs and subarch ribs are connected by steel box cross-braces. The bowed height is 32.5m and the ratio of rise to span is 1:4. The cross sections of the main arch ribs and subarch ribs are varying in the longitudinal direction. There are 19 cables hanged between the steel girder and the arch ribs, which are made of parallel galvanized high tensile steel wires with a diameter of 5mm and protected by the package of two layers of polyethylene. The width of the deck is changed from 46.5m to 52.5m in the longitudinal direction. The lane arrangement is composed of a two-way six-lane in the middle and two non-motor vehicle lanes on two sides. The cross-sectional and elevation drawings of the arch bridge are shown in Figs. 15 and 16.

4.2 Measurement of displacement influence lines

Upon the completion of the bridge construction, the field loading tests were carried out before the bridge is opened to public traffic. The displacement influence lines of key positions at the bridge deck have been acquired during the passing of heavy vehicles on different traffic lanes. Presented in this paper are the results of displacement influence lines measured by the vision-based system when a heavy vehicle moves on the lane 1, as illustrated in Fig. 15. The heavy vehicle is employed to produce a moving load with different velocities and its total weight is 400kN. The details of the heavy vehicle are shown in Fig. 17. As illustrated in Fig. 18, three vision targets (P1, P2 and P3) were deployed on the bridge deck at the locations of 1/2, 3/8 and 1/4 of the main span of the arch bridge. The vision-based system synchronously recorded the displacement time histories of the three targets when the heavy vehicle is moving along the lane 1 on the deck with a certain velocity and direction, as listed in Table 3. The dynamic displacement is measured by the structural dynamic displacement measurement method based on the GPM algorithm.

Fig. 14 Site photo of arch bridge

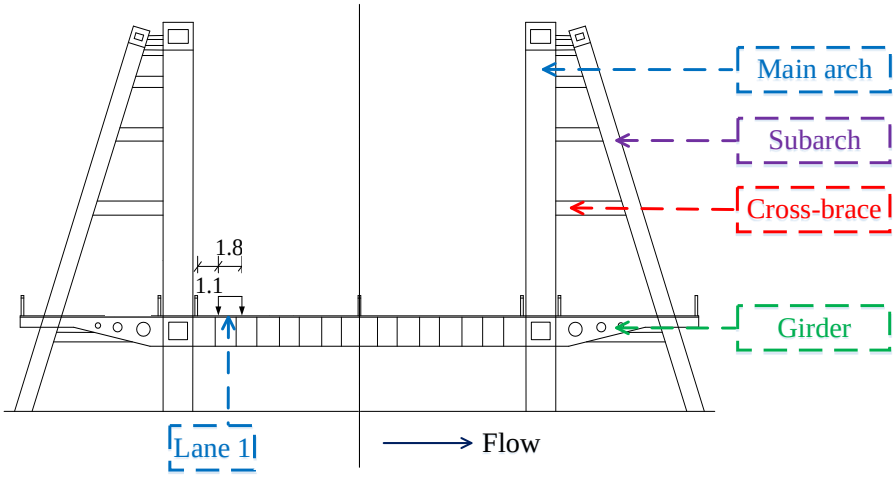

Fig. 15 Cross-sectional view of arch bridge

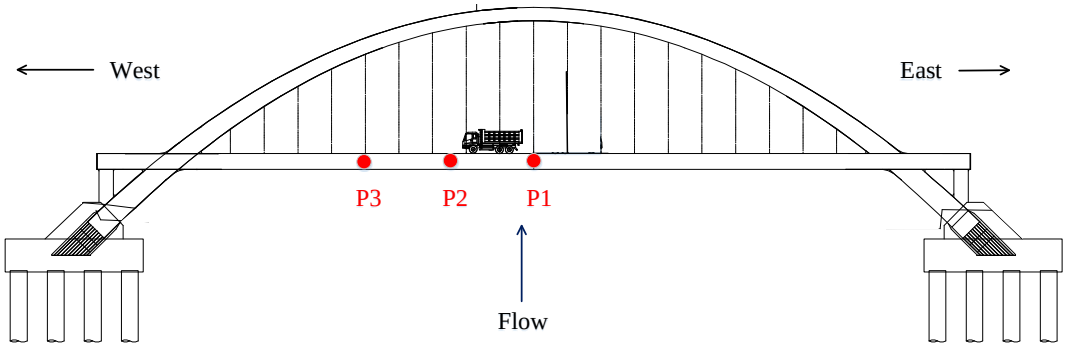

Fig. 16 Elevation view of arch bridge

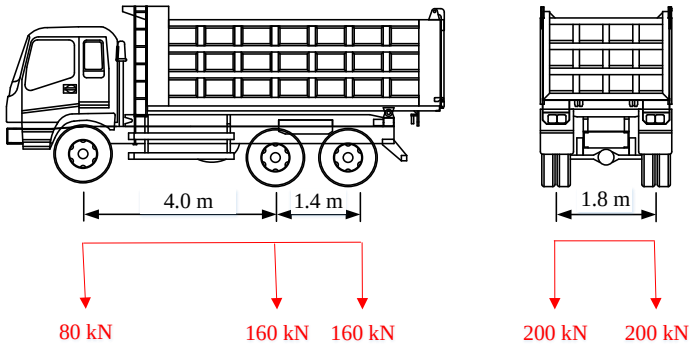

Fig. 17 Details of heavy vehicle

Fig. 18 Experimental setup of field experiments

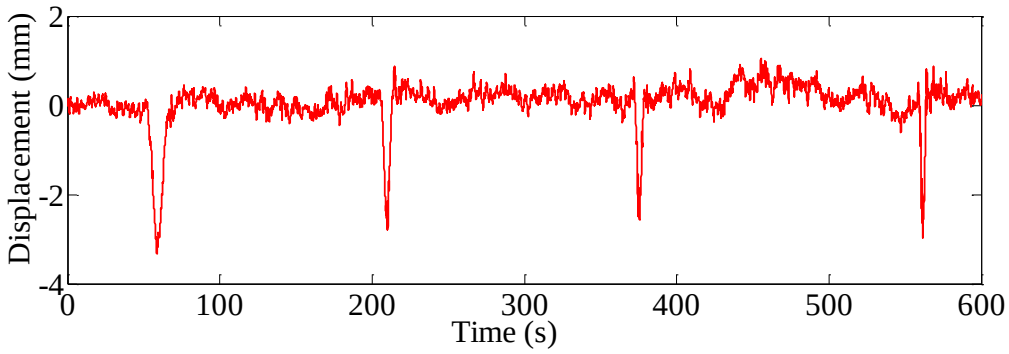

Fig. 19 Measured displacement time histories of P1 under moving load

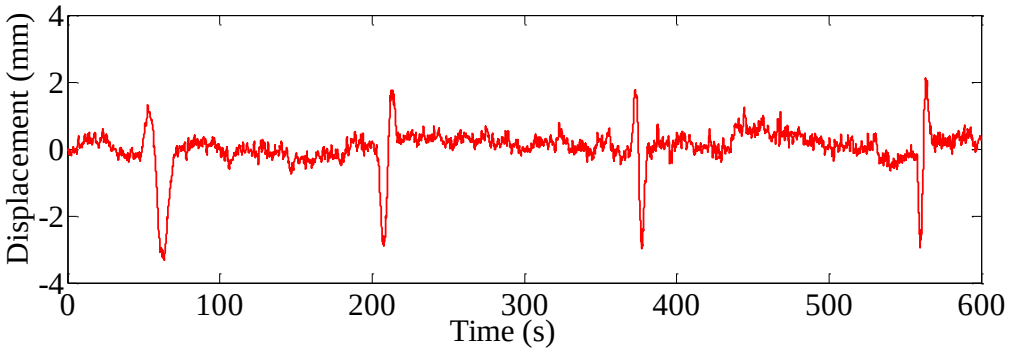

Fig. 20 Measured displacement time histories of P2 under moving load

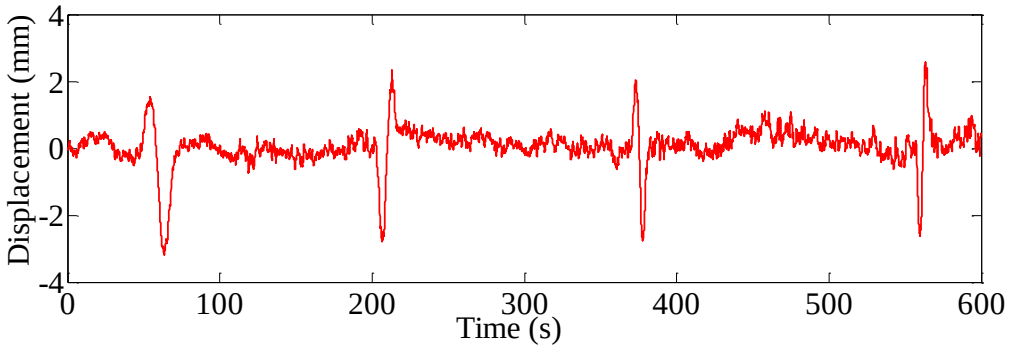

Fig. 21 Measured displacement time histories of P3 under moving load

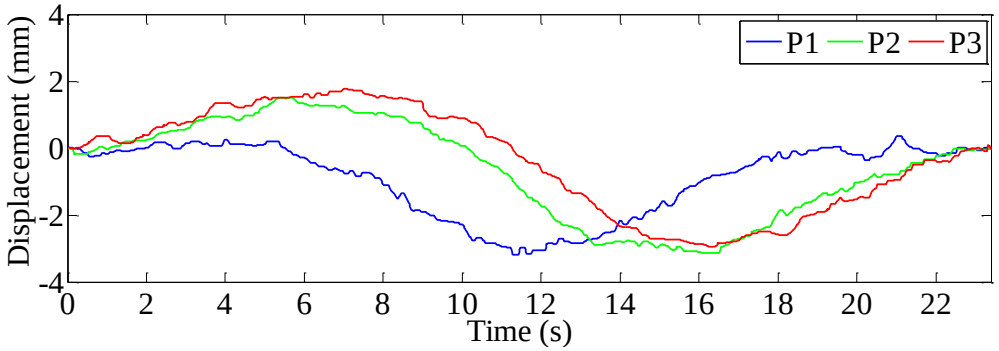

Fig. 22 Measured displacement influence lines of three vision points of Case 10

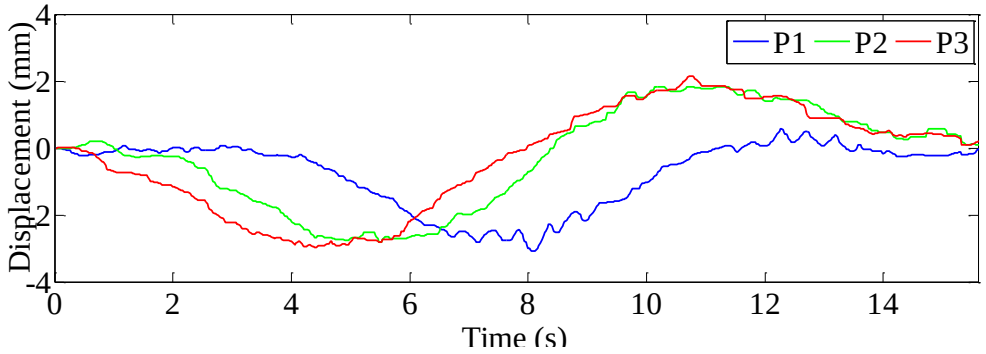

Fig. 23 Measured displacement influence lines of three vision points of Case 11

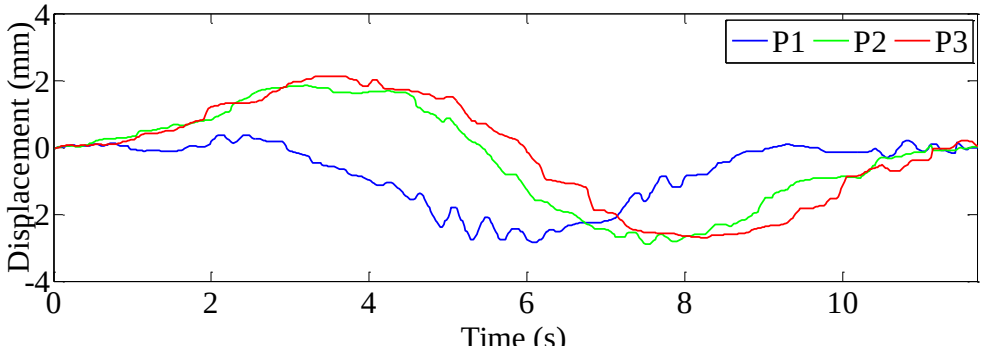

Fig. 24 Measured displacement influence lines of three vision points of Case 12

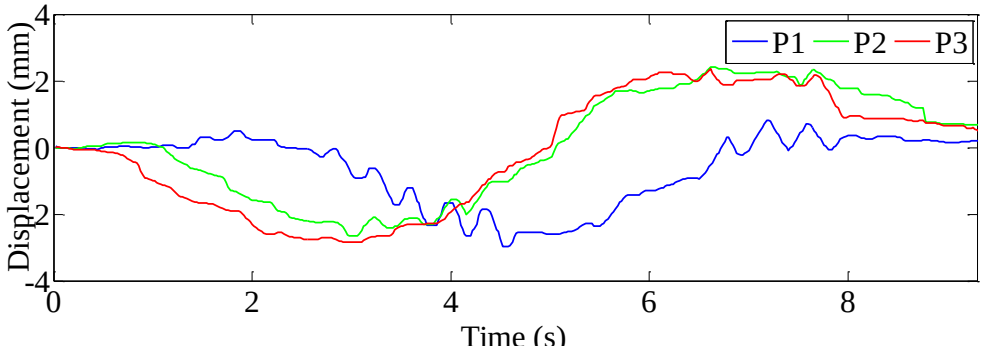

Fig. 25 Measured displacement influence lines of three vision points of Case 13

Table 3 Cases for measurement of displacement influence lines

Case No.	Moving velocity (km/h)	Direction
Case 10	20	From east to west
Case 11	30	From west to east
Case 12	40	From east to west
Case 13	50	From west to east

Figs. 19-21 illustrate the displacement influence lines of the three deployment points measured by the vision-based system for the four cases. It is revealed that when the heavy vehicle is passing near the position of the vision point, the structural displacement reaches the maximum value. Figs. 22-25 illustrate the measured displacement influence lines of the three vision points on the bridge deck for the four cases. It is seen from Figs. 22-25 that if the moving direction of the heavy vehicle is changed, the sequence of the maximum value of the structural displacement will be different.

5. Conclusions

This study addressed the methodology and experimental verification of a vision-based system for structural dynamic displacement measurement based on three different kinds of image processing algorithms, i.e., the grayscale pattern matching (GPM) algorithm, the color pattern matching (CPM) algorithm, and the mean shift tracking (MST) algorithm. The comparative analysis results of the experiments show that the three image processing algorithms have good capability and stability for structural dynamic displacement measurement of multiple points referring to the results simultaneously measured by the magnetostrictive displacement sensor (MDS). The effectiveness of the vision-based system was also validated through measurement of the displacement influence lines of an arch bridge during the loading tests. In the future work, the research will be focused on the robustness and adaptability of each image processing algorithm for structural dynamic displacement measurement under various adverse conditions such as unfavorable environmental factors (e.g., wind, rain and fog) and surrounding ground vibration. Furthermore, field experiments will be carried out to investigate the advantages and disadvantages of each image processing algorithm under different types of application scenarios.

Acknowledgments

The work described in this paper was jointly supported by the National Science Foundation of China (Grant Nos. 51308493 and U1234204) and the Research Fund for the Doctoral Program of Higher Education of China (Grant No. 20130101120080).

References

Cheng, Y.Z. (1995), "Mean shift, mode seeking, and clustering", *IEEE T. Pattern. Anal.*, **17**(8), 790-799.

Comaniciu, D., Ramesh, V. and Meer, P. (2003), "Kernel-based object tracking", *IEEE T. Pattern. Anal.*, **25**(5), 564-577.

Feng, D.M., Feng, M.Q., Ozer, E. and Fukuda, Y. (2015), "A vision-based sensor for noncontact structural displacement measurement", *Sensors*, **15**, 16557-16575.

Fukuda, Y., Feng, M.Q., Narita, Y., Kaneko, S.I. and Tanaka, T. (2013), "Vision-based displacement sensor for monitoring dynamic response using robust object search algorithm", *IEEE Sens. J.*, **13**(12), 4725-4732.

Fukunaga, K. and Hostetler, L.D. (1975), "The estimation of the gradient of a density function, with application in pattern recognition", *IEEE T. Inform. Theory*, **21**(1), 32-40.

Guo, J. and Zhu, C.A. (2016), "Dynamic displacement measurement of large-scale structures based on the Lucas–Kanade template tracking algorithm", *Mech. Syst. Signal. Pr.*, **66-67**, 425-436.

Henke, K., Pawlowski, R., Schregle, P. and Winter, S. (2015), "Use of digital image processing in the monitoring of deformations in building structures", *J. Civil Struct. Health Monit.*, **5**, 141-152.

Ho, H.N., Lee, J.H., Park, Y.S. and Lee, J.J. (2012), "A synchronized multipoint vision-based system for displacement measurement of civil infrastructures", *Sci. World J.*, **2012**, 519146.

Jauregui, D.V., White, K.R., Woodward, C.B. and Leitch, K.R. (2003), "Noncontact photogrammetric measurement of vertical bridge deflection", *J. Bridge Eng. - ASCE*, **8**(4), 212-222.

Ji. Y.F. and Chang, C.C. (2007), "Nontarget stereo vision technique for spatiotemporal response measurement of line-like structures", *J Eng Mech- ASCE*. **134**(6), 466-474.

Ji. Y.F. and Chang, C.C. (2008), "Nontarget image-based technique for small cable vibration measurement", *J. Bridge Eng. - ASCE*, **13**(1), 34-42.

Mansoori, E.G., Zolghadri, M.J. and Katebi, S.D. (2007), "A weighting function for improving fuzzy classification systems performance", *Fuzzy Set Syst.*, **158**, 583-591.

Ni, Y.Q., Ye, X.W. and Ko, J.M. (2010), "Monitoring-based fatigue reliability assessment of steel bridges: analytical model and application", *J. Struct. Eng. - ASCE*, **136**(12), 1563-1573.

Ni, Y.Q., Ye, X.W. and Ko, J.M. (2012), "Modeling of stress spectrum using long-term monitoring data and finite mixture distributions", *J. Eng. Mech. - ASCE*, **138**(2), 175-183.

Olaszek, P. (1999), "Investigation of the dynamic characteristic of bridge structures using a computer vision method", *Measurement*, **25**, 227-236.

Park, J.W., Lee, J.J., Jung. H.J. and Myung, H. (2010), "Vision-based displacement measurement method for high-rise building structures using partitioning approach", *NDT&E Int.*, **43**, 642-647.

Perlibakas, V. (2004), "Distance measures for PCA-based face recognition", *Pattern Recogn. Lett.*, **25**, 711-724.

Russell, S.J. and Norvig, P. (2010), *Artificial Intelligence: A Modern Approach*, 3rd Ed, Pearson Prentice Hall, Upper Saddle River, NJ.

Wahbeh, A.M., Caffrey, J.P. and Masri, S.F. (2003), "A vision-based approach for the direct measurement of displacements in vibrating systems", *Smart Mater. Struct.*, **12**, 785-794.

Ye, X.W., Ni, Y.Q., Wai, T.T., Wong, K.Y., Zhang, X.M. and Xu, F. (2013), "A vision-based system for dynamic displacement measurement of long-span bridges: algorithm and verification", *Smart Struct. Syst.*, **12**(3-4), 363-379.

Ye, X.W., Ni, Y.Q., Wong, K.Y. and Ko, J.M. (2012), "Statistical analysis of stress spectra for fatigue life assessment of steel bridges with structural health monitoring data", *Eng. Struct.*, **45**, 166-176.

Ye, X.W., Yi, T.H., Dong, C.Z., Liu, T. and Bai, H. (2015), "Multi-point displacement monitoring of bridges using a vision-based approach", *Wind Struct.*, **20**(2), 315-326.